Accurate Density Functional Theory for Non-Covalent Interactions in Charged Systems

Heng Zhao,[1] Balázs D. Lőrincz,[2,3,4] Tobias Henkes,[5] Dénes Berta,[2,3,4]
Péter R. Nagy,[2,3,4] Alexandre Tkatchenko,[5] and Stefan Vuckovic[1,*]

[1] *Department of Chemistry, University of Fribourg, Fribourg, Switzerland.*
[2] *Department of Physical Chemistry and Materials Science, Faculty of Chemical Technology and Biotechnology, Budapest University of Technology and Economics, Műegyetem rkp. 3., H-1111 Budapest, Hungary*
[3] *HUN-REN–BME Quantum Chemistry Research Group, Műegyetem rkp. 3., H-1111 Budapest, Hungary*
[4] *MTA–BME Lendület Quantum Chemistry Research Group, Műegyetem rkp. 3., H-1111 Budapest, Hungary*
[5] *Department of Physics and Materials Science, University of Luxembourg, Luxembourg City, Luxembourg.*

Accurately modeling non-covalent interactions (NCIs) involving charged systems remains an outstanding challenge in Density Functional Theory (DFT), with implications across natural and life sciences, engineering, e.g., in biochemistry, catalysis, and materials science. For these interactions, the interplay between electrostatics, polarization, and dispersion leads to systematic errors of up to tens of kcal/mol in standard dispersion-enhanced DFT methods. We solve this problem by introducing (r^{2}SCAN+MBD)@HF, a DFT method without empirically fitted parameters that combines the r^{2}SCAN functional and many-body dispersion, both evaluated on Hartree-Fock densities.

I. INTRODUCTION

Non-covalent interactions (NCIs) involving charged systems (charged NCIs for simplicity) are ubiquitous across scientific disciplines, such as in acid-base, electro-, redox-, coordination chemistry, ionic crystals and liquids, ionization and electron attachment processes, charge conduction and transfer, etc. For example, in biology, charged NCIs stabilize enzymatic transition states [1], mediate protein folding via salt bridges between charged amino acid side chains [2], and regulate ion transport [3]. In catalysis, ionic complex stability dictates reaction pathways and selectivity, (e.g., in Brønsted and Lewis acid catalysis [4]). In materials science, they enable gas separation in metal-organic frameworks (MOFs) [5] and play a crucial role in the design of batteries by governing alkali metal intercalation in electrode materials [6]. Thus, accurate computational models of charged NCIs are essential, spanning applications from ionic liquids [7] to electrochemical processes in energy storage systems [8].

When it comes to computational simulations of NCIs, including those involving charged species, benchmark-level accuracy is typically achieved using high-level wavefunction-based methods, such as Coupled Cluster with Single, Double, and perturbative Triple excitations [CCSD(T)] [9] and Quantum Diffusion Monte Carlo (DMC) [10]. Despite advances in cost-reduction [11–14], these wavefunction methods remain impractical for biological or condensed-phase systems exceeding hundreds of atoms.

The unparalleled trade-off between accuracy and cost has made Density Functional Theory (DFT) the workhorse for NCI simulations [15–17]. While DFT initially struggled with dispersion interactions, this issue has been largely mitigated, especially for neutral cases, by various dispersion methods [18–26]. However, the growing interest in charged NCI datasets [27–29], including the extensive DES15K benchmark set [30], has revealed the major limitations of dispersion-enhanced DFT for these interactions [17]. Namely, while dispersion-enhanced DFT typically performs well for neutral complexes, with interaction energy errors around 0.5 kcal/mol, its errors for charged species can be up to 10 times larger, regardless of the chosen method ("D3" [21, 22], "D4" [31, 32], "XDM" [18, 19], "TS" [20], or "MBD" [25, 26]). This issue is systematic, as recently demonstrated by Johnson's study of ∼15k [30] NCI complexes [17].

Computational simulations of charged NCIs fundamentally differ from neutral ones, especially for interactions between metallic cations and neutral molecules. A prototypical example is the Li^+–benzene complex [17], where the strong inhomogeneous electric field from Li^+'s localized positive charge distorts the benzene electron cloud, inducing partial electron transfer. From the perspective of the theory of intermolecular interactions, describing such interactions in inhomogeneous electric fields is notoriously challenging, as electrostatics, polarization, and dispersion become inherently coupled [33]. This coupling critically influences a broad range of (bio)chemical processes, such as selectivity in biological ion channels (see Ref. [3]). Further complexity arises because external charges substantially alter dispersion interactions, stabilizing or destabilizing molecular binding depending on the charge sign [33].

Within DFT, accurately describing strongly polarized complexes under electric fields is particularly challenging due to delocalization errors—often termed "the greatest outstanding challenge in DFT" [34]. Another critical issue is accurately capturing electrostatics, polarization, and dispersion and their coupling, requiring care-

* stefan.vuckovic@unifr.ch

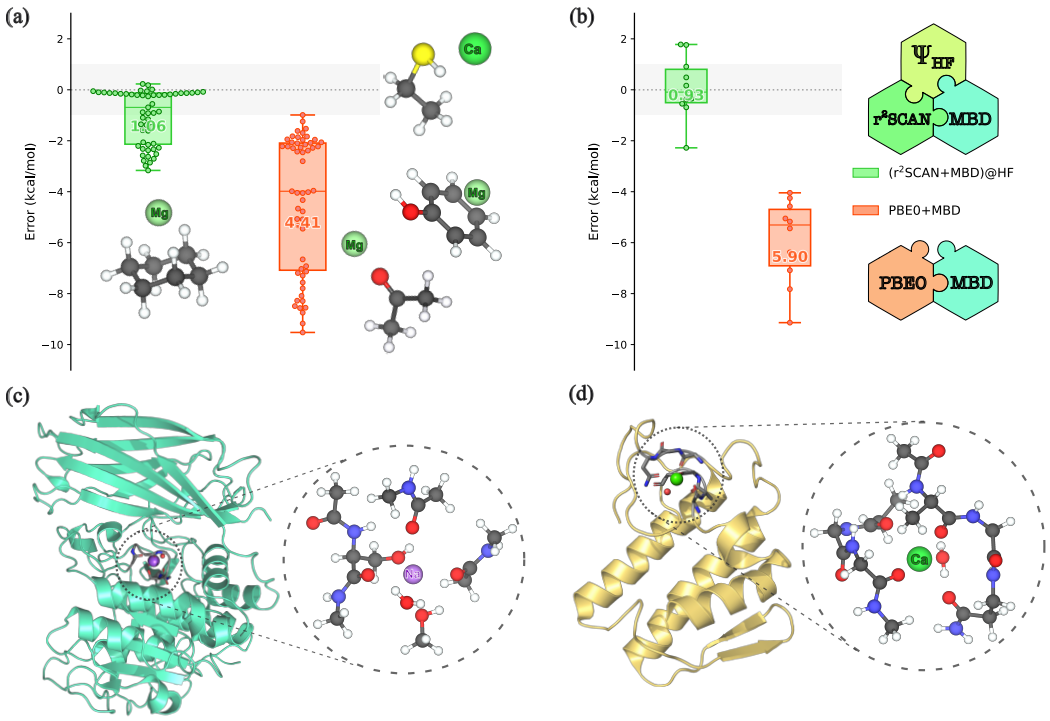

FIG. 1: Beeswarm and boxplots with the interaction energy errors (kcal/mol) of (r^{2}SCAN+MBD)@HF and PBE0+MBD methods for earth alkaline dication complexes in (a) DES15K and (b) MIPC datasets, with numbers in the middle of the boxes denoting the mean absolute errors. Cartoon representations of proteins (c) 7O20 and (d) 1POD from the MIPC dataset, with zoomed-in views of their curated cluster structures. The labels for panels (c, d) correspond to Protein Data Bank (PDB) identifiers.

ful balancing of short- and long-range correlation without double-counting effects [35, 36]. Along these lines, dispersion methods in DFT compensate for the long-range correlation missed by (semi-local) DFT approximations [15–17]. However, dispersion methods must be balanced with base DFT to avoid double-counting of correlation effects (see Refs. 35 and 36). Although general, this issue is particularly severe for charged NCIs, due to the interplay of polarization, density errors, and poor transferability of dispersion methods trained on neutral NCIs. Simply put, DFT typically underbinds neutral NCIs, so dispersion methods improve their interaction energies. In contrast, for charged NCIs, where DFT already overbinds, adding an attractive dispersion energy only worsens the overbinding. Thus, developing a dispersion-enhanced DFT approximation that describes both neutral and charged NCIs remains a major challenge.

Resolving this challenge with charged NCIs is crucial, especially today as machine-learning force fields (MLFFs) trained on DFT data expand the reach of DFT quality modeling to larger systems and longer dynamics simulations [37]. However, any errors in DFT propagate to MLFFs, reducing their reliability and predictive power [38–40]. Given the critical role of charged NCIs across many applications and the growing use of MLFFs to extend DFT's reach [41], it is imperative to address DFT's deficiencies in describing these interactions.

In this work, we solve the DFT problem of charged NCIs by ensuring a balanced description of correlation effects in both neutral and charged systems through the integrative development of (r^{2}SCAN+MBD)@HF. In (r^{2}SCAN+MBD)@HF, the r^{2}SCAN functional and many-body dispersion (MBD) are evaluated on the Hartree-Fock (HF) orbitals—a combination essential for ensuring a consistent and accurate treatment of both neutral and charged NCIs. Beyond solving the problem of charged NCIs, our integrative design of (r^{2}SCAN+MBD)@HF yields several key advantages over existing dispersion-enhanced DFT methods. **(1)** It achieves a balanced treatment of short- and long-range correlations across diverse NCIs, which is missed by other dispersion-enhanced DFT approximations. **(2)** With minimal empiricism (only one MBD parameter, set to unity and largely system-insensitive), we avoid extensive empirical fitting of dispersion methods, which can be highly sensitive to the training set [42–44] and limit method transferability [45]. **(3)** Despite being designed to address the DFT deficiencies for charged NCIs, our method retains robust accuracy

for neutral systems, matching or surpassing leading semilocal and hybrid functionals on main-group benchmarks. Furthermore, using HF densities within the "density- and dispersion-corrected DFT" framework of Sim, Burke, and co-workers [42–44] serves a dual purpose in (r^{2}SCAN+MBD)@HF: while HF densities typically improve upon approximate DFT densities for charged NCIs, their primary role here is to maintain balance between baseline DFT and MBD across different NCI types. Crucially, this balance is lost if DFT's self-consistent density is used (e.g., if r^{2}SCAN+MBD is employed in place of (r^{2}SCAN+MBD)@HF); more broadly, altering any of its three components disrupts the consistent description of neutral and charged NCIs, typically leading to severe overbinding of charged complexes.

By addressing DFT's deficiencies for charged NCIs while retaining accuracy for neutral systems, (r^{2}SCAN+MBD)@HF provides a robust framework for quantum simulations of complex NCIs. The most challenging examples from our benchmark sets that include earth dications, ranging from small complexes to clusters extracted from our Metal Ion Protein Clusters dataset (see Results), are shown in Fig. 1 and illustrate major and consistent improvements of (r^{2}SCAN+MBD)@HF over the widely used PBE0+MBD method. As demonstrated in Results through the consistent success of (r^{2}SCAN+MBD)@HF for charged NCIs, our method is ideally suited for computational studies in fields where charged NCIs are critical, including biomolecular interactions, adsorption in MOFs, and electrode materials in batteries.

II. RESULTS

(r^{2}SCAN+MBD)@HF Resolves Charged NCI Issues: DES15K insights

Figure 2 highlights a central finding of this work, demonstrating how (r^{2}SCAN+MBD)@HF significantly improves dispersion-enhanced DFT accuracy for charged NCIs. We assess (r^{2}SCAN+MBD)@HF on the DES15K dataset ($\approx$ 15,000 dimers spanning neutral and charged complexes) [30]. Specifically, Fig. 2 presents error distribution histograms for interaction energies in different DES15K categories, comparing (r^{2}SCAN+MBD)@HF to the widely used PBE0+MBD. While many other DFT+dispersion combinations could be considered, it is crucial to note that Johnson and co-workers have shown that dispersion methods systematically fail for charged NCIs [17], leading to large errors regardless of the method used. For this reason, we focus on comparing (r^{2}SCAN+MBD)@HF with PBE0+MBD, which is not only representative of the performance of dispersion-enhanced DFT for charged NCIs [17] but also a widely adopted in recent molecular dataset generation efforts [46, 47].

Figs. 2(a) and 2(b) illustrate the most striking improvements of (r^{2}SCAN+MBD)@HF for charged NCIs. For alkaline earth dication–neutral complexes (Fig. 2a), PBE0+MBD severely overbinds (MAE = 4.41 kcal/mol), while (r^{2}SCAN+MBD)@HF reduces this error by a factor of four and yielding much less skewed error distribution. Similarly, for alkali cation–neutral complexes (Fig. 2b), (r^{2}SCAN+MBD)@HF reduces the MAE compared to PBE0+MBD (1.91 kcal/mol) by a factor of three, again resulting in a significantly less skewed error distribution. These results highlight (r^{2}SCAN+MBD)@HF's robustness in correcting DFT failures for NCIs with cations.

Fig. 2(c) includes less polarizing non-metal cations with more delocalized charges interacting with neutral molecules. Consequently, PBE0+MBD yields smaller errors (MAE = 1.08 kcal/mol) than in Fig. 2(a,b). Yet, (r^{2}SCAN+MBD)@HF still significantly improves accuracy, reducing the MAE nearly by half (to 0.60 kcal/mol), further demonstrating its robustness for charged NCIs.

We now turn to another DES15K subset: anion–neutral complexes. Fig. 2(d) shows that both methods perform similarly for non-metal anion–neutral pairs, with PBE0+MBD slightly outperforming (r^{2}SCAN+MBD)@HF (MAE = 0.6 vs. 0.8 kcal/mol). However, (r^{2}SCAN+MBD)@HF is generally more robust for anion-containing NCIs because (i) semilocal DFT often yields unphysical results for anions with positive HOMO energies that imply unbound states[48], hence the red flag next to PBE0+MBD in Fig. 2(d); and (ii) for more challenging cases like the B30 dataset[49], (r^{2}SCAN+MBD)@HF reduces the MAE by half compared to PBE0+MBD (Tab. S3).

For cation–anion pairs (Fig. 2e), dominated by strong electrostatics, PBE0+MBD again significantly overbinds (MAE = 1.39 kcal/mol). (r^{2}SCAN+MBD)@HF substantially improves accuracy (MAE = 0.76 kcal/mol), with most errors within $\pm$2 kcal/mol. For neutral complexes (Fig. 2f), where PBE0+MBD already performs well [17], (r^{2}SCAN+MBD)@HF remains comparably accurate (MAE $\sim$ 0.5 kcal/mol).

These results demonstrates the robustness of (r^{2}SCAN+MBD)@HF, highlighting its success in addressing dispersion-corrected DFT deficiencies for charged NCIs. Additionally, despite its minimally empirical nature, (r^{2}SCAN+MBD)@HF matches the performance of modern dispersion-corrected semilocal and hybrid functionals on the diverse organic GMTKN55 dataset (Tab. S4) [50], further emphasizing its robustness. In the following sections, we explore practical applications to metal-containing protein interactions and analyze the principles underlying (r^{2}SCAN+MBD)@HF's improved accuracy.

(r^{2}SCAN+MBD)@HF at work for metal-protein interactions

Having established the accuracy of (r^{2}SCAN+MBD)@HF for DES15k, we now assess it on biologically relevant metal–protein interactions. To this end, we have curated the Metal Ion Protein Clusters

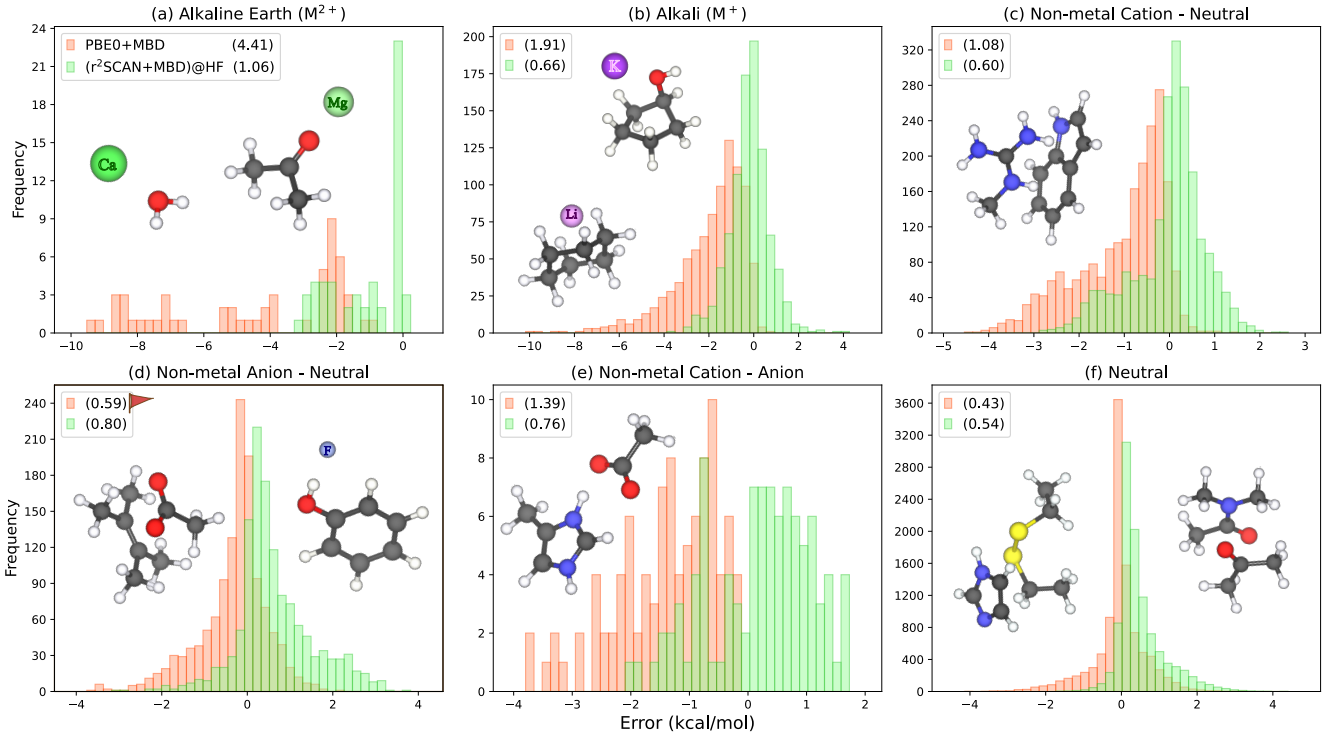

FIG. 2: Histograms of error distribution for interaction energy predictions using (r^2SCAN+MBD)@HF and PBE0+MBD methods for different subsets of DES15K dataset: (a) Alkaline earth dication complexes, (b) Alkali cation complexes, (c) Non-metal cation-neutral complexes, (d) Non-metal anion-neutral complexes, with the red flag indicating general and specific challenges of self-consistent DFT for anions (see text); (e) Non-metal cation-anion complexes, and (f) Neutral complexes. Numbers in parentheses represent corresponding mean absolute errors (MAEs) in kcal/mol. Negative errors indicate overbinding, while positive errors indicate underbinding.

(a)

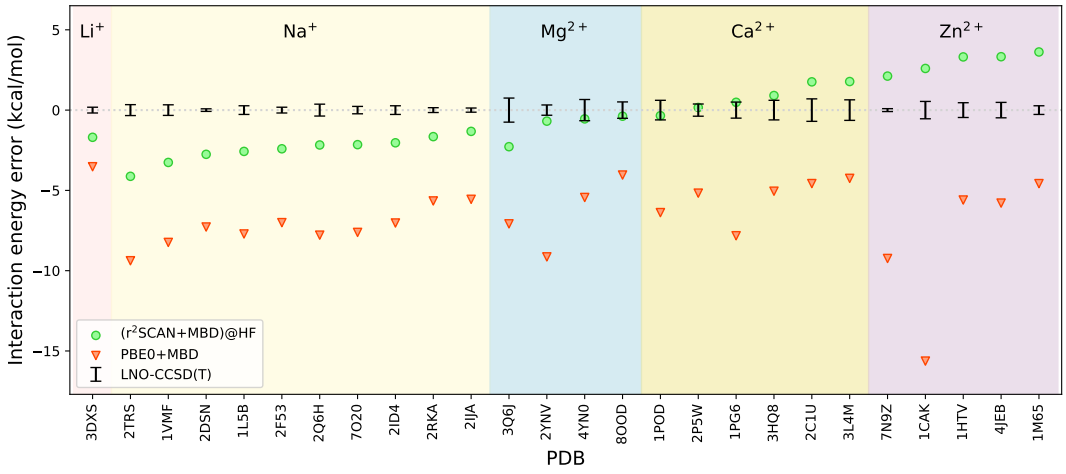

FIG. 3: Comparison of the interaction energy errors of (r^2SCAN+MBD)@HF and PBE0+MBD methods for the MIPC dataset, labeled by their PDB codes. Black error bars indicate uncertainty estimates of the LNO-CCSD(T) reference (see Methods). Representative protein structures (cartoon) and corresponding metal–ligand clusters (ball-and-stick) are shown in Fig. 1.

(MIPC) dataset, consisting of 25 biologically relevant metal–ligand complexes extracted from high-resolution

Protein Data Bank (PDB) crystal structures with metal cations coordinated by neutral amino acid residues.

In our MIPC, examples include catalytic ion sites, e.g., the secondary Ca^{2+} site in Phospholipase A_2 (PDB ID 1POD) [51] or one of the Zn^{2+} ions of the zinc-cluster in the YcdX (PDB ID 1M65), setting up a hydroxide nucleophile for phosphoesther hydrolysis [52]. In other cases present in MIPC, the ion binding is linked to allosteric regulation of substrate binding (PDB IDs 2C1U, 7O20) [53, 54]. In an inhibitor screening study for sodium-coupled transporter LeuT (PDB ID 2Q6H) [55], sodium sites are in the close proximity of binding site of the leucine and the inhibitor clomipramine. The reliable computation of such binding energies is especially important when the identification of the bound cation relies on quantum-mechanical calculations (PDB ID 2DSN) [56].

For each protein in MIPC, we construct a cluster model by selecting amino acid residues within the first coordination shell of metal ions (Li^+, Na^+, Mg^{2+}, Ca^{2+}, and Zn^{2+}). We then benchmark the interaction energies between metallic cation and its surrounding amino acid residues using high-level LNO-CCSD(T) calculations [12, 13, 57, 58] and include benchmark uncertainty estimates (see Methods).

Fig. 3 compares (r^2SCAN+MBD)@HF and PBE0+MBD errors against LNO-CCSD(T) reference interaction energies for MIPC (including uncertainty estimates). Systems are grouped by metal cation and labeled by PDB codes, with representative proteins (cartoon) and corresponding metal–ligand clusters (ball-and-stick) from MIPC illustrated in Fig. 1.

Fig. 3 shows that the excellent performance of (r^2SCAN+MBD)@HF for charged NCIs extends to MIPC (MAE = 1.82 kcal/mol), whereas PBE0+MBD consistently overbinds MIPC systems (MAE = 6.72 kcal/mol). Furthermore, for nearly all main-group dication systems (Ca^{2+}, Mg^{2+}), (r^2SCAN+MBD)@HF shows errors within reference uncertainty. For alkali metal cations Na^+ and Li^+ (selected for therapeutic relevance [59]), (r^2SCAN+MBD)@HF remains consistently superior to PBE0+MBD. For the protein clusters with Zn^{2+}, a closed-shell transition metal cation also absent from DES15K, the same trend is observed. MIPC represents a significant step to real-life systems also in terms of the coverage of the ions with ligands: ions in MIPC are coordinated with 4–6 lingands. This introduces several challenges for MIPC simulations. First, ion–ligand interaction errors naturally grow with the number of ligands. Second, modeling polarized ligand–ligand interactions is difficult, as they often become overly repulsive due to overpolarization in previous DFT methods, an issue that (r^2SCAN+MBD)@HF effectively overcomes.

These results demonstrate that (r^2SCAN+MBD)@HF reliably describes such complex charged interactions when ions placed into realistic protein or solvent environments. For example, these are critical to biological functions such as substrate binding, catalytic activity, and allosteric regulation. Its robust accuracy across diverse charged NCIs makes (r^2SCAN+MBD)@HF a powerful method for biochemical simualtions.

The role of densities in (r^2SCAN+MBD)@HF for cation-neutral pairs

Having demonstrated (r^2SCAN+MBD)@HF's accuracy for charged NCIs, we now analyze how it outperforms standard dispersion-enhanced DFT. A natural question arises: is this success primarily due to the r^2SCAN functional, the MBD term, or the use of HF densities? Analyzing the contributions of these components individually and combined, we find that (r^2SCAN+MBD)@HF's accuracy relies on their synergy—altering any component disrupts this balance and compromises accuracy for charged and/or neutral NCIs.

We first examine the role of HF densities in (r^2SCAN+MBD)@HF. It has been shown that evaluating functionals on the HF densities, instead of self-consistent ones, often significantly improves DFT accuracy across many systems [43, 44, 48, 60, 61]. For certain systems (e.g., stretched heterodimers), HF densities are more accurate (i.e., energetically closer) to their exact counterparts than DFT ones. leading to DFT evaluated on HF densities improving over self-consistent DFT *for the right reason* [62]. However, for other systems, such as transition states, whether this improvement for the right reason or error cancellations has been questioned [63, 64].

Thus, to determine whether HF or DFT densities are more accurate for our systems of interest, we compare both against high-quality CCSD densities for representative cation–neutral complexes in Fig. 4. Specifically, for metallic cation-neutral molecule pairs, we analyze the spherically averaged deformation density, $\Delta\tilde{\rho}(\mathbf{r}, u)$, which isolates changes in electron distribution upon complex formation. Second, by placing $\mathbf{r}$ at the metal cation, $\Delta\tilde{\rho}(\mathbf{r}, u)$ reveals how electron density redistributes—accumulating or depleting—around the metal cation as a function of radial distance u, providing a spherically averaged view of polarization effects. To define $\Delta\tilde{\rho}(\mathbf{r}, u)$, we first introduce the spherically averaged electron density, $\tilde{\rho}(\mathbf{r}, u)$ (see Methods for a precise definition), which represents the average electron density at a distance u from a reference point $\mathbf{r}$ [65–67]. Then, $\Delta\tilde{\rho}(\mathbf{r}, u)$ is defined as the difference between $\tilde{\rho}(\mathbf{r}, u)$ of the complex and the sum of those from its isolated fragments (the cation and the neutral molecule). Importantly, $\Delta\tilde{\rho}(\mathbf{r}, u)$ integrates to zero at every $\mathbf{r}$, $\int_0^\infty du\, 4\pi u^2 \Delta\tilde{\rho}(\mathbf{r}, u) = 0$.

Figure 4 shows $4\pi u^2 \Delta\tilde{\rho}(\mathbf{r}, u)$ for selected cation-neutral complexes computed at the CCSD, PBE0, and HF levels, with $\mathbf{r}$ placed at the cation. We also display CCSD isosurfaces of $\Delta\rho(\mathbf{r})$ (the usual deformation, i.e., interaction density) to visualize charge redistributions. For panels (a) water - K^+ and (b) chlorobenzene - K^+, the HF (spherically averaged deformation) densities more closely match CCSD results than PBE0, supporting their use in (r^2SCAN+MBD)@HF. The results for more systems follow similar trends and are given

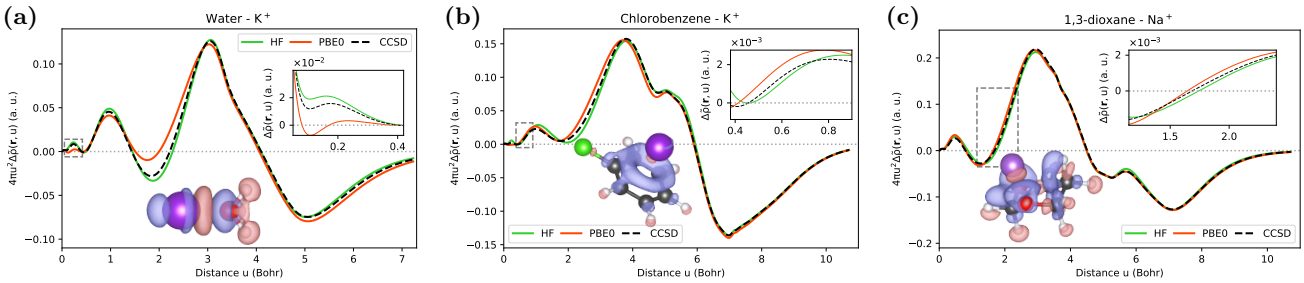

FIG. 4: (a) Spherically averaged deformation density, $\Delta\tilde{\rho}(\mathbf{r}, u)$ (see Methods) for the H_2O–K^+ complex calculated using HF, PBE0, and CCSD methods, in which $\mathbf{r}$ placed at the position of the K^+ nucleus. Inset shows a zoom-in of this quantity in the highlighted (boxed) u region. The other inset shows the standard deformation density, $\Delta\rho(\mathbf{r})$, visualized as a 3D isosurface (isovalue 3.0×10^{-4} e/bohr^3) (b, c) Same as in (a), but for chlorobenzene-K^+ and 1,3-dioxane-Na^+, respectively.

in Figs. S3 and S4. However, in panel (c) 1,3-dioxane-Na^+, we cannot clearly determine whether HF or PBE0 is more accurate. While this analysis confirms that the HF (deformation) densities are more accurate than those of PBE0 for our cation–neutral complexes, it alone does not fully explain why (r^{2}SCAN+MBD)@HF achieves its overall accuracy. Beyond improving density accuracy for charged NCIs, the HF densities also play a key role in (r^{2}SCAN+MBD)@HF's success by restoring the balance between the r^{2}SCAN and MBD contributions to interaction energies, a critical aspect explored in the next section.

The accuracy of (r^{2}SCAN+MBD)@HF- the synergy of the three components

To demonstrate the synergy of its three components in achieving high accuracy for both neutral and charged NCIs, Fig. 5 shows dissociation curves for three prototypical NCI-bound complexes. In this figure, DFT methods are benchmarked against CCSD(T) references for: (a) Li^+–benzene (cation–neutral interaction), (b) acetic acid dimer (hydrogen-bonded), and (c) benzene dimer (dispersion-bound π–π stacking). In Fig. 5, the top row compares (r^{2}SCAN+MBD)@HF with PBE0-based variants, while the bottom row compares it with r^{2}SCAN-based variants, highlighting that altering any of the three components in (r^{2}SCAN+MBD)@HF compromises its accuracy.

An essential requirement for a base DFT functional is that it underbinds NCIs, allowing the dispersion term to properly compensate this underbinding (see Ref. 35 for a more formalized criterion using the concept of "dispersionless" functionals). For example, PBE0 correctly underbinds the benzene dimer (Fig. 5(c), top), allowing MBD to improve its binding. However, it already overbinds the Li^+–benzene complex (Fig. 5(a), top), so adding MBD only exacerbates the error. Thus, PBE0 fails to meet the fundamental requirement for dispersion-enhanced DFT: a base functional that consistently underbinds complexes across diverse NCIs, enabling dispersion corrections to accurately compensate.

On the other hand, self-consistent r^{2}SCAN exhibits the desired underbinding behavior for the complexes in Fig. 5(a, c) [bottom], but not for the hydrogen-bonded acetic acid dimer in Fig. 5(b) [bottom], where it shows excessive overbinding, a behavior previously observed in Ref. 43 for hydrogen-bonded systems. Among the three base functionals used here, only r^{2}SCAN evaluated on the HF density (r^{2}SCAN@HF) exhibits a consistent underbinding trend across the three prototypical systems for the three NCI types. The interaction energies are significantly improved once dispersion is restored through adding our MBD term to r^{2}SCAN@HF. This highlights the critical synergy among the three components (r^{2}SCAN, MBD, and HF density) in (r^{2}SCAN+MBD)@HF, enabling balanced accuracy across diverse NCIs—an essential feature not achieved by other combinations.

Now, we turn to the role of dispersion in (r^{2}SCAN+MBD)@HF, which is more subtle. Previously, r^{2}SCAN@HF combined with the D4 correction and density-corrected (DC) parameters, yielding r^{2}SCAN@HF-DC4, achieved excellent general accuracy, especially for hydrogen-bonded complexes and water [43]. Consistent with this, r^{2}SCAN@HF-DC4 performs well for neutral complexes [Figs. 5(b,c), bottom], but notably fails for the Li^+–benzene system [Fig. 5(a), bottom]. This failure arises due to the sensitivity of the r^{2}SCAN@HF-DC4 results to both the density and its D4 empirical parameters [42, 43] for the cation-neutral pairs. To elaborate on this, we have to go into more technical details on the construction of the dispersion methods. Namely, both MBD and D4 rely (at least indirectly) on the density information, with the latter requiring partial atomic charges for its construction [32]. By default settings, classical partial atomic charges trained on the DFT density data are used in D4 [32]. Since these settings are used in both the training and application of r^{2}SCAN@HF-DC4, this method still retains input from the DFT densities, even though it is designed for the HF densities. On top of the indirect DFT density input, the classical charges employed in the D4 part of r^{2}SCAN@HF-

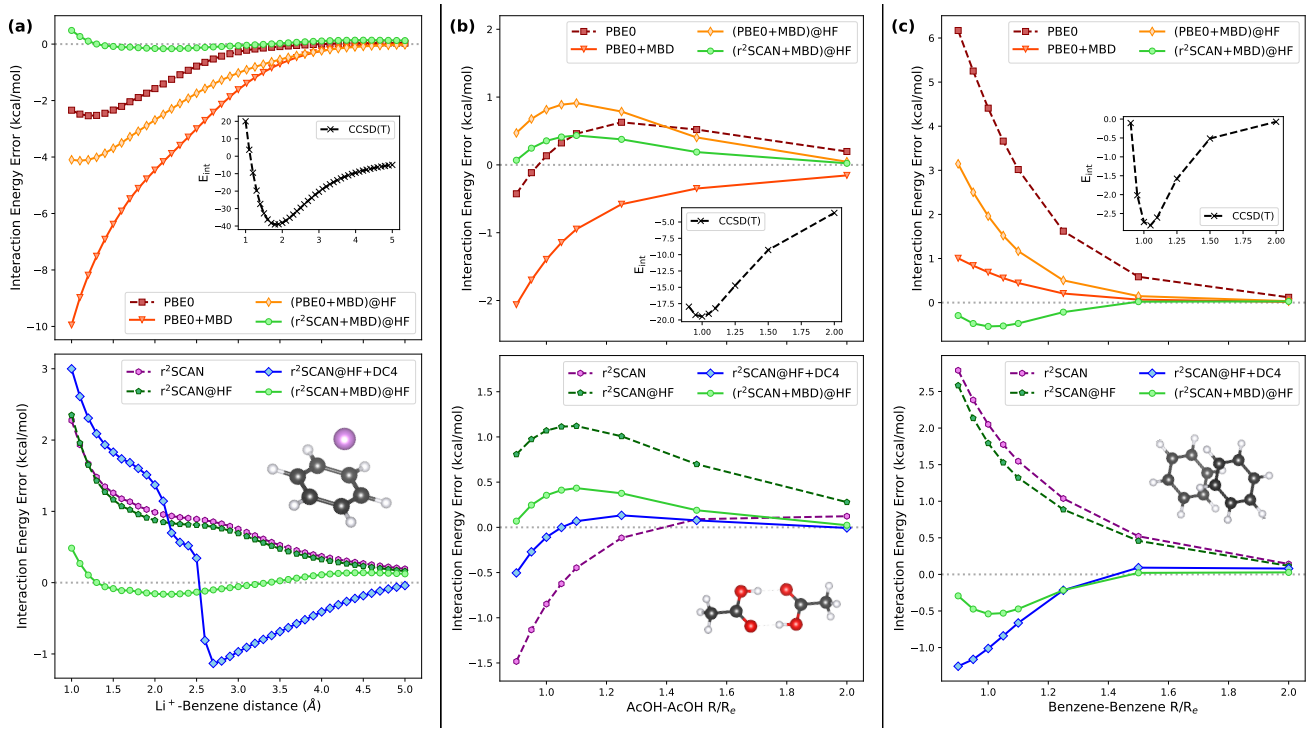

FIG. 5: Errors in computed interaction energies relative to CCSD(T) reference data (interaction curves shown as insets, upper panels) for: (a) Li^+–benzene as a function of cation-benzene distance (Å); (b) acetic acid dimer; (c) benzene dimer, each as a function of separation normalized to equilibrium distance (R/R_e). Upper panels show errors progressing from bare PBE0, adding MBD (PBE0+MBD), using density-corrected version ((PBE0+MBD)@HF), to finally (r^{2}SCAN+MBD)@HF. Lower panels similarly progress from bare r^{2}SCAN, density-corrected r^{2}SCAN@HF, previously reported r^{2}SCAN@HF+DC4, to (r^{2}SCAN+MBD)@HF. As we progress along this sequence of functionals towards (r^{2}SCAN+MBD)@HF, the interaction energy errors systematically decrease.

DC4 are based on the so-called *electronegativity equilibration* model, which inherently suffers from artificial long-range charge transfer, especially for systems containing ions [68]. In contrast to these problems present in r^{2}SCAN@HF-DC4, (r^{2}SCAN+MBD)@HF strictly computes both the functional and the MBD term on the HF densities without any input from the DFT densities. Moreover, (r^{2}SCAN+MBD)@HF is nearly non-empirical, with its only empirical parameter β, which controls the range-separation of MBD interaction, set to unity. Crucially, when coupled with r^{2}SCAN@HF, MBD@HF exhibits remarkable insensitivity to β variations across different systems, as we will show later.

Transforming r^{2}SCAN@HF's initial weakness into (r^{2}SCAN+MBD)@HF's key strength

In Fig. 2, we have shown that (r^{2}SCAN+MBD)@HF success for charged NCIs is due to the complementarity between MBD and r^{2}SCAN@HF, with MBD accurately compensating for r^{2}SCAN@HF's systematic underbinding. This ensures balanced accuracy across both charged and neutral NCIs, a key advantage of (r^{2}SCAN+MBD)@HF over other dispersion-enhanced methods. What enables this balance is the consistent underbinding behavior of r^{2}SCAN@HF, as observed previously for prototypical complexes across different NCIs. Here we further demonstrate that this critical behavior of r^{2}SCAN@HF—essential for (r^{2}SCAN+MBD)@HF's success (Figs. 2, 3, 5)—is systematic, using the broader DES15K dataset. Fig. 6(a) compares signed interaction energy errors from r^{2}SCAN@HF, PBE0@HF, and PBE0 across neutral (left) and metal cation–neutral complexes (right). Only r^{2}SCAN@HF consistently underbinds both neutral and cation complexes, unlike PBE0-based methods. As a result, only r^{2}SCAN@HF, among the three methods, can be transformed into an accurate dispersion-enhanced DFT approach by adding a dispersion term. In this way, the systematic underbinding by r^{2}SCAN@HF, initially a weakness, becomes (r^{2}SCAN+MBD)@HF's key strength when combined with MBD, enabling balanced accuracy for charged and neutral NCIs.

Completing the Puzzle: How MBD Enables (r^{2}SCAN+MBD)@HF's Accuracy

Now, we examine the final piece of the puzzle—MBD's role in (r^{2}SCAN+MBD)@HF's success. MBD has only one empirical parameter, β, which we set to unity in (r^{2}SCAN+MBD)@HF. Increasing β weakens MBD contribution to interaction energies, vanishing as $\beta \to \infty$. Figure 6(b) shows how the interaction energy for the

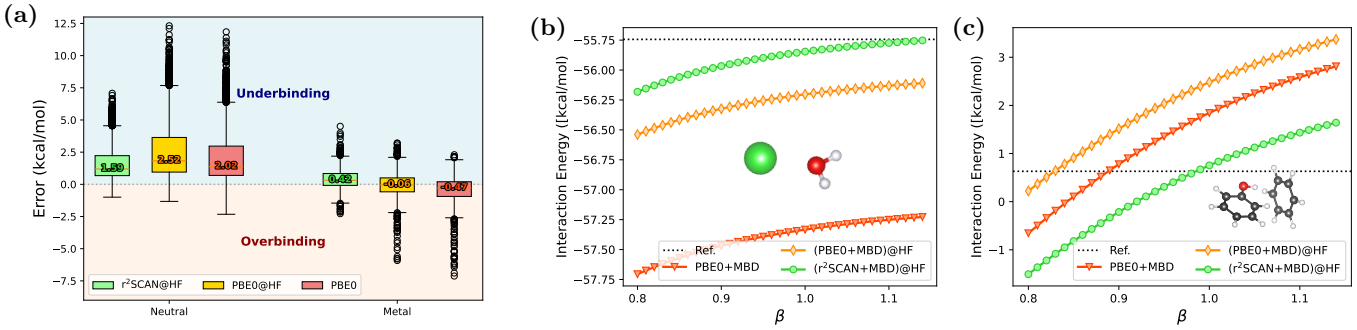

FIG. 6: (a) Boxplot of interaction energy errors (kcal/mol) for r^{2}SCAN@HF, PBE0@HF, and PBE0 across Neutral and Metal subsets of DES15K. Boxes show interquartile ranges, medians (lines), outliers (circles), and mean errors (numbers). (b, c) Dependence of DFT+MBD interaction energies on the MBD parameter β for (b) H_2O–Ca^{2+} and (c) benzene–phenol complexes. Reference interaction energies (CCSD(T)) are indicated by dotted lines.

H_2O–Ca^{2+} complex depends on the MBD parameter β for r^{2}SCAN@HF, PBE0, and PBE0@HF, with the reference energy indicated by the horizontal dashed line. For (r^{2}SCAN+MBD)@HF (green curve), the optimal β is slightly above 1, making our choice of $\beta = 1$ nearly optimal. In contrast, since PBE0 and PBE0@HF already overbind the complex, their β-curves never cross the reference line, instead favoring large β values (ideally $\beta \to \infty$) to suppress further overbinding from MBD.

A stark contrast appears in Fig. 6(c) for the neutral benzene–phenol complex. Here, PBE0 and PBE0@HF require smaller β values (0.8–0.9) to match the reference—unlike the large β values favored previously (Fig. 6(b)). Remarkably, (r^{2}SCAN+MBD)@HF again aligns closely with the reference at $\beta \approx 1$ (also optimal for the full neutral NCI dataset, S22 [69]), highlighting its excellent consistency across charged and neutral NCIs.

Further analysis in the SI, covering additional systems (Fig. S2) and transferability tests of DFT+MBD trained on neutral NCIs and evaluated on charged NCIs and vice versa (Fig. S1) confirms the results of Figs. 6(b,c). Only when using r^{2}SCAN@HF as a baseline does DFT+MBD exhibit consistently small sensitivity to β across different NCIs, allowing (r^{2}SCAN+MBD)@HF to simultaneously maintain high accuracy for both neutral and charged interactions. In contrast, the greater sensitivity of other methods implies improving accuracy for one interaction type inevitably reduces it for the other. Thus, (r^{2}SCAN+MBD)@HF's unique β-insensitivity makes it ideal for simulations of systems where different interaction types coexist, such as biomolecular complexes (e.g., Fig. 3).

DISCUSSION

Accurate yet tractable quantum-mechanical treatment of charged NCIs remains a key challenge with broad implications from biochemistry to materials. Dispersion-enhanced DFT has major difficulties in describing charged NCIs due to the interplay of density errors, coupling of polarization and dispersion, and the poor transferability of dispersion corrections trained on neutral systems. Improving charged NCIs accuracy without compromising neutral ones cannot be solved by merely adding charged systems to the dispersion method training. Instead, as we show here, it requires a foundational solution that balances correlation effects for both neutral and charged NCIs. Specifically, achieving this balance requires a dispersion method to accurately compensate for what the base DFT misses, which is easier for neutral NCIs but becomes highly nontrivial for charged ones. Restoring this balance is central to the integrative design of (r^{2}SCAN+MBD)@HF for accurate treatment of both charged and neutral NCIs. Crucially, altering any of its three components (r^{2}SCAN, MBD, or HF densities) breaks this balance.

A distinguishing feature of (r^{2}SCAN+MBD)@HF is its overall minimal empiricism, (i.e., it is free from empirical parameters fitted to data) reflected in each of its three components. Despite this, (r^{2}SCAN+MBD)@HF improves accuracy for charged NCIs, maintains performance for neutral NCIs, and achieves accuracy comparable to leading semi-local functionals on main-group benchmarks (GMTKN55). This broader accuracy enables (r^{2}SCAN+MBD)@HF to support applications from biochemistry to materials, where charged NCIs coexist with other interactions. For example, in biochemistry, accurate simulations of enzymatic reactions with a metallic cation in the active site require capturing both cation affinity and reaction kinetics [70, 71]. These challenges often couple when cations stabilize transition states, as with Mg^{2+} in kinase-catalyzed phosphoryl transfers [70, 71]. Thus, describing such systems requires a method that can capture both reaction barriers and NCIs involving the cation, making (r^{2}SCAN+MBD)@HF a strong candidate for advancing enzymatic simulations.

On the materials side, an example of interactions be-

tween metallic cations and neutral gases is the challenging adsorption of small molecules on open-metal-site (OMS) MOFs [72], which is another target for future applications of (r^{2}SCAN+MBD)@HF. These systems are hard to simulate as classical force fields are unreliable near the OMS [73], and the recently developed MLFFs for MOFs display limitations due to the DFT training data [74]. We expect that this problem can be addressed by training MLFFs on (r^{2}SCAN+MBD)@HF data. More broadly, (r^{2}SCAN+MBD)@HF can serve as a general-purpose DFT method for generating high-quality reference data to train MLFFs, particularly for charged systems, with (r^{2}SCAN+MBD)@HF's forces implemented following Refs [75, 76].

METHODS

DFT Calculations. All DFT calculations were performed using `pySCF` package [77]. For DES15K calculations, we used def2-QZVPPD basis set [78], RI approximations are used with corresponding auxiliary basis sets [79] to accelerate the calculation. For MIPC calculations, we used def2-TZVPD basis set [78], while for Ca and Zn complexes in MIPC, we used aug-cc-pVTZ [80] for other elements, and aug-cc-pVTZ-PP [81] for Ca and Zn with MCDHF-ECP-10 pseudopotential [82]. The base functional r^{2}SCAN@HF and PBE0@HF energies were evaluated on converged HF densities. The default grid level 5 in `pySCF` was used for all HF-DFT calculations. The MBD calculation were performed on HF densities using libMBD package [83]. The empirical range-separation parameter $\beta = 1.0$ in MBD@rsSCS [26] was selected for all calculations. The high-level reference data for Li^+-benzene dissociation curve were reported in Ref 17. The reference data of other dissociation curves in Fig 5 are from S66x8 database [84].

Spherically averaged density that we used in Fig. 4 is defined as,

$$\tilde{\rho}(\mathbf{r}, u) = \frac{1}{4\pi} \int_0^{\pi} \int_0^{2\pi} \rho(\mathbf{r} + \mathbf{u}) \sin\phi \, d\theta \, d\phi,$$

and it satisfies

$$4\pi \int_0^{\infty} \tilde{\rho}(\mathbf{r}, u) \, u^2 \, du = N,$$

where N is the number of electrons.

The integrand $4\pi u^2 \tilde{\rho}(\mathbf{r}, u)$ is defined as radial density.

Spherically averaged deformation density is defined as

$$\Delta\tilde{\rho}(\mathbf{r}, u) = \tilde{\rho}_{\mathrm{AB}}(\mathbf{r}, u) - \tilde{\rho}_{\mathrm{A}}(\mathbf{r}, u) - \tilde{\rho}_{\mathrm{B}}(\mathbf{r}, u),$$

and

$$4\pi \int_0^{\infty} \Delta\tilde{\rho}(\mathbf{r}, u) \, u^2 \, du = 0.$$

MIPC Clusters Creation.

The MIPC protein structures have been extracted from PDB and then completed with explicit hydrogen atoms by using CHARMM-GUI [85]. To create protein-ion clusters (i.e. cation with surounding amino acid residues), we have made initial selection of atoms within 5 Å of the ion. Then, we have iteratively extended this selection until aliphatic C-C bonds could be cut and capped with hydrogens. This approach ensured that the first coordination shell of the ion sites were included with minimum system size while keeping the edge of the QM selection as indifferent as possible.

LNO-CCSD(T) reference interaction energies CCSD (T) reference calculations were performed with our linear-scaling local natural orbital (LNO) CCSD(T) [12, 13, 57, 58] method in the Mrcc [86–88] program suite. To accelerate the convergence towards the complete basis set (CBS) limit, we combine basis set extrapolation, counterpoise correction [89] and density-based basis set correction (DBBSC) [90]. The CBS and local approximation free (LAF) limit of CCSD(T) is estimated for the MIPC set as

$$E_{\mathrm{CCSD(T)}} = E^{\mathrm{TZ,DBBSC}}_{\mathrm{N-T\ LNO}} - E^{\mathrm{TZ,DBBSC}}_{\mathrm{Normal\ LNO}} + E^{\mathrm{CBS(T,Q),DBBSC}}_{\mathrm{Normal\ LNO}}. \quad (1)$$

Here, superscripts XZ refer to the cardinal number X of the aug-cc-pV(X+d)Z basis sets [91], while the corresponding CBS extrapolated values are denoted as CBS(X,$X+1$) [92]. Subscripts `Normal` (N) and `Tight` (T) denote LNO thresholds, while N–T denotes LAF extrapolation towards canonical CCSD(T) using `Normal` and `Tight` LNO settings. [12, 13] The system specific uncertainty estimates corresponding to Eq. (1), plotted in Fig. 3, are the sum of uncertainty estimates for the basis set and LNO approximations. These are obtained, respectively, as the size of the DBBSC correction at the CBS(T,Q) level and via the LAF framework [12, 13] as $\pm 0.5(E^{\mathrm{TZ,DBBSC}}_{\mathrm{Tight\ LNO}} - E^{\mathrm{TZ,DBBSC}}_{\mathrm{Normal\ LNO}})$. This level of convergence provides, on the average, about ±0.5 kcal/mol uncertainty for the LNO-CCSD(T) interaction energies of the MIPC set. An additional benefit of the composite Eq. (1), in addition to its robust and low uncertainty estimate, is its computational cost. The required LNO-CCSD(T) computations took about 1–2 days of wall time with few 10s of CPU cores and ca. 50 GBs of minimal memory requirement for the complexes of 40–70 atoms. LNO-CCSD(T) for the largest, 90–110 atom complexes required about twice as much resource. The reliability of the CCSD(T) estimate of Eq. (1) is extensively validated against even better converged LNO-CCSD(T) results for 5 representative protein-ion complexes (see the last section of Supplementary Information for additional details).

III. ACKNOWLEDGMENTS

Funding: S.V. and H.Z. acknowledge funding from the SNSF Starting Grant project (TMSGI2_211246).

B.D.L. and P.R.N. acknowledge funding of the János Bolyai Research Scholarship of the Hungarian Academy of Sciences and the ERC Starting Grant No. 101076972, "aCCuracy". D.B. and P.R.N. acknowledge support by the National Research, Development, and Innovation (NRDI) Office (Starting 149434, FK142489). A.T. acknowledges the ERC Advanced Grant "FITMOL". T.H. acknowledges an AFR grant from the Luxembourg National Research Fund. The Hungarian Governmental Information-Technology Development Agency is acknowledged for awarding access to the Komondor and the LEONARDO supercomputer, owned by the EuroHPC Joint Undertaking, hosted by CINECA (Italy) and the LEONARDO consortium.

Authors contributions: H.Z. and S.V. formulated the project. H.Z. performed all DFT calculations. B.D.L. and P.R.N. performed the LNO-CCSD(T) calculations on the MIPC dataset. T.H. and D.B. curated the the MIPC dataset. H.Z., B.D.L., T.H., D.B., P.R.N., A.T., and S.V. wrote the manuscript with input from all authors. S.V., P.R.N., and A.T. supervised the project.

Competing interests: The authors declare no other competing interests.

[1] V. A. Adhav and K. Saikrishnan, *Acs Omega*, 2023, **8**, 22268–22284.
[2] R. W. Newberry and R. T. Raines, *ACS chemical biology*, 2019, **14**, 1677–1686.
[3] M. Rossi, A. Tkatchenko, S. B. Rempe and S. Varma, *Proceedings of the National Academy of Sciences*, 2013, **110**, 12978–12983.
[4] S. Yamada, *Chemical reviews*, 2018, **118**, 11353–11432.
[5] G. Maurin, C. Serre, A. Cooper and G. Férey, *Chemical Society Reviews*, 2017, **46**, 3104–3107.
[6] J.-X. Huang, G. Csányi, J.-B. Zhao, J. Cheng and V. L. Deringer, *Journal of Materials Chemistry A*, 2019, **7**, 19070–19080.
[7] K. Fumino, S. Reimann and R. Ludwig, *Physical Chemistry Chemical Physics*, 2014, **16**, 21903–21929.
[8] B. Huang, S. Muy, S. Feng, Y. Katayama, Y.-C. Lu, G. Chen and Y. Shao-Horn, *Physical Chemistry Chemical Physics*, 2018, **20**, 15680–15686.
[9] J. Rezac and P. Hobza, *Journal of chemical theory and computation*, 2013, **9**, 2151–2155.
[10] W. M. Foulkes, L. Mitas, R. Needs and G. Rajagopal, *Reviews of Modern Physics*, 2001, **73**, 33.
[11] C. Riplinger and F. Neese, *The Journal of chemical physics*, 2013, **138**, 034106.
[12] P. R. Nagy and M. Kállay, *J. Chem. Theory Comput.*, 2019, **15**, 5275.
[13] P. R. Nagy, *Chem. Sci.*, 2024, **15**, 14556.
[14] A. Zen, J. G. Brandenburg, J. Klimeš, A. Tkatchenko, D. Alfè and A. Michaelides, *Proceedings of the National Academy of Sciences*, 2018, **115**, 1724–1729.
[15] S. Grimme, A. Hansen, J. G. Brandenburg and C. Bannwarth, *Chemical reviews*, 2016, **116**, 5105–5154.
[16] P. Xu, M. Alkan and M. S. Gordon, *Chemical Reviews*, 2020, **120**, 12343–12356.
[17] C. J. Nickerson, K. R. Bryenton, A. J. Price and E. R. Johnson, *The Journal of Physical Chemistry A*, 2023, **127**, 8712–8722.
[18] E. R. Johnson and A. D. Becke, *The Journal of chemical physics*, 2006, **124**, 174104.
[19] A. D. Becke and E. R. Johnson, *The Journal of chemical physics*, 2007, **127**, 154108.
[20] A. Tkatchenko and M. Scheffler, *Physical review letters*, 2009, **102**, 073005.
[21] S. Grimme, J. Antony, S. Ehrlich and H. Krieg, *The Journal of chemical physics*, 2010, **132**, 154104.
[22] S. Grimme, S. Ehrlich and L. Goerigk, *Journal of computational chemistry*, 2011, **32**, 1456–1465.
[23] J. Klimeš, D. R. Bowler and A. Michaelides, *Journal of Physics: Condensed Matter*, 2009, **22**, 022201.
[24] O. A. Vydrov and T. Van Voorhis, *The Journal of chemical physics*, 2010, **133**, 244103.
[25] A. Tkatchenko, R. A. DiStasio Jr, R. Car and M. Scheffler, *Physical review letters*, 2012, **108**, 236402.
[26] A. Ambrosetti, A. M. Reilly, R. A. DiStasio and A. Tkatchenko, *The Journal of chemical physics*, 2014, **140**, 18A508.
[27] S. Spicher, E. Caldeweyher, A. Hansen and S. Grimme, *Physical Chemistry Chemical Physics*, 2021, **23**, 11635–11648.
[28] V. Wineman-Fisher, Y. Al-Hamdani, P. R. Nagy, A. Tkatchenko and S. Varma, *The Journal of Chemical Physics*, 2020, **153**, 094115.
[29] I. Sandler, S. Sharma, B. Chan and J. Ho, *The Journal of Physical Chemistry A*, 2021, **125**, 9838–9851.
[30] A. G. Donchev, A. G. Taube, E. Decolvenaere, C. Hargus, R. T. McGibbon, K.-H. Law, B. A. Gregersen, J.-L. Li, K. Palmo, K. Siva *et al.*, *Scientific data*, 2021, **8**, 55.
[31] E. Caldeweyher, S. Ehlert, A. Hansen, H. Neugebauer, S. Spicher, C. Bannwarth and S. Grimme, *The Journal of chemical physics*, 2019, **150**, 154122.
[32] E. Caldeweyher, J.-M. Mewes, S. Ehlert and S. Grimme, *Physical Chemistry Chemical Physics*, 2020, **22**, 8499–8512.
[33] A. Kleshchonok and A. Tkatchenko, *Nature communications*, 2018, **9**, 3017.
[34] K. R. Bryenton, A. A. Adeleke, S. G. Dale and E. R. Johnson, *WIREs Computational Molecular Science*, 2023, **13**, e1631.
[35] K. Pernal, R. Podeszwa, K. Patkowski and K. Szalewicz, *Physical review letters*, 2009, **103**, 263201.
[36] A. J. Price, K. R. Bryenton and E. R. Johnson, *The Journal of Chemical Physics*, 2021, **154**, 230902.
[37] O. T. Unke, M. Stöhr, S. Ganscha, T. Unterthiner, H. Maennel, S. Kashubin, D. Ahlin, M. Gastegger, L. Medrano Sandonas, J. T. Berryman *et al.*, *Science Advances*, 2024, **10**, eadn4397.
[38] O. T. Unke, S. Chmiela, H. E. Sauceda, M. Gastegger, I. Poltavsky, K. T. Schutt, A. Tkatchenko and K.-R. Müller, *Chemical Reviews*, 2021, **121**, 10142–10186.
[39] P. Montero de Hijes, C. Dellago, R. Jinnouchi and G. Kresse, *The Journal of Chemical Physics*, 2024, **161**, 131102.

[40] E. Palos, E. Lambros, S. Swee, J. Hu, S. Dasgupta and F. Paesani, *Journal of Chemical Theory and Computation*, 2022, **18**, 3410–3426.

[41] T. W. Ko, J. A. Finkler, S. Goedecker and J. Behler, *Nature communications*, 2021, **12**, 398.

[42] S. Song, S. Vuckovic, E. Sim and K. Burke, *The journal of physical chemistry letters*, 2021, **12**, 800–807.

[43] S. Song, S. Vuckovic, Y. Kim, H. Yu, E. Sim and K. Burke, *Nature communications*, 2023, **14**, 799.

[44] M. Lee, B. Kim, M. Sim, M. Sogal, Y. Kim, H. Yu, K. Burke and E. Sim, *Journal of Chemical Theory and Computation*, 2024, **20**, 7155–7167.

[45] T. Gould, B. Chan, S. G. Dale and S. Vuckovic, *Chemical Science*, 2024.

[46] J. Hoja, L. Medrano Sandonas, B. G. Ernst, A. Vazquez-Mayagoitia, R. A. DiStasio Jr and A. Tkatchenko, *Scientific data*, 2021, **8**, 43.

[47] L. Medrano Sandonas, D. Van Rompaey, A. Fallani, M. Hilfiker, D. Hahn, L. Perez-Benito, J. Verhoeven, G. Tresadern, J. Kurt Wegner, H. Ceulemans *et al.*, *Scientific Data*, 2024, **11**, 742.

[48] M.-C. Kim, E. Sim and K. Burke, *Physical review letters*, 2013, **111**, 073003.

[49] A. Bauza, I. Alkorta, A. Frontera and J. Elguero, *Journal of chemical theory and computation*, 2013, **9**, 5201–5210.

[50] L. Goerigk, A. Hansen, C. Bauer, S. Ehrlich, A. Najibi and S. Grimme, *Physical Chemistry Chemical Physics*, 2017, **19**, 32184–32215.

[51] D. L. Scott, S. P. White, J. L. Browning, J. J. Rosa, M. H. Gelb and P. B. Sigler, *Science*, 1991, **254**, 1007–1010.

[52] A. Teplyakov, G. Obmolova, P. P. Khil, A. J. Howard, R. D. Camerini-Otero and G. L. Gilliland, *Proteins: Structure, Function, and Bioinformatics*, 2003, **51**, 315–318.

[53] A. Echalier, C. F. Goodhew, G. W. Pettigrew and V. Fülöp, *Structure*, 2006, **14**, 107–117.

[54] S. O. Dahms, T. Haider, G. Klebe, T. Steinmetzer and H. Brandstetter, *ACS Chemical Biology*, 2021, **16**, 1692–1700.

[55] S. K. Singh, A. Yamashita and E. Gouaux, *Nature*, 2007, **448**, 952–956.

[56] H. Matsumura, T. Yamamoto, T. C. Leow, T. Mori, A. B. Salleh, M. Basri, T. Inoue, Y. Kai and R. N. Z. R. A. Rahman, *Proteins: Structure, Function, and Bioinformatics*, 2008, **70**, 592–598.

[57] P. R. Nagy and M. Kállay, *J. Chem. Phys.*, 2017, **146**, 214106.

[58] P. R. Nagy, G. Samu and M. Kállay, *J. Chem. Theory Comput.*, 2018, **14**, 4193.

[59] V. Wineman-Fisher, J. M. Delgado, P. R. Nagy, E. Jakobsson, S. A. Pandit and S. Varma, *The Journal of Chemical Physics*, 2020, **153**, 104113.

[60] E. Sim, S. Song, S. Vuckovic and K. Burke, *Journal of the American Chemical Society*, 2022, **144**, 6625–6639.

[61] S. Song, S. Vuckovic, E. Sim and K. Burke, *Journal of chemical theory and computation*, 2022, **18**, 817–827.

[62] S. Nam, S. Song, E. Sim and K. Burke, *Journal of chemical theory and computation*, 2020, **16**, 5014–5023.

[63] A. D. Kaplan, C. Shahi, P. Bhetwal, R. K. Sah and J. P. Perdew, *Journal of Chemical Theory and Computation*, 2023, **19**, 532–543.

[64] B. Kanungo, A. D. Kaplan, C. Shahi, V. Gavini and J. P. Perdew, *The Journal of Physical Chemistry Letters*, 2024, **15**, 323–328.

[65] H. Bahmann, Y. Zhou and M. Ernzerhof, *The Journal of Chemical Physics*, 2016, **145**, 124104.

[66] S. Vuckovic and P. Gori-Giorgi, *The Journal of Physical Chemistry Letters*, 2017, **8**, 2799–2805.

[67] S. Vuckovic and H. Bahmann, *Journal of Chemical Theory and Computation*, 2023, **19**, 6172–6184.

[68] T. Froitzheim, M. Müller, A. Hansen and S. Grimme, 2025.

[69] P. Jurečka, J. Šponer, J. Černý and P. Hobza, *Phys. Chem. Chem. Phys.*, 2006, **8**, 1985–1993.

[70] R. Recabarren, K. Zinovjev, I. Tuñón and J. Alzate-Morales, *ACS Catalysis*, 2020, **11**, 169–183.

[71] K. Nam, A. R. A. Thodika, S. Tischlik, C. Phoeurk, T. M. Nagy, L. Schierholz, J. Ådén, P. Rogne, M. Drescher, A. E. Sauer-Eriksson and M. Wolf-Watz, *Science Advances*, 2024, **10**, eado5504.

[72] U. Kökçam-Demir, A. Goldman, L. Esrafili, M. Gharib, A. Morsali, O. Weingart and C. Janiak, *Chemical Society Reviews*, 2020, **49**, 2751–2798.

[73] A. L. Dzubak, L.-C. Lin, J. Kim, J. A. Swisher, R. Poloni, S. N. Maximoff, B. Smit and L. Gagliardi, *Nature Chemistry*, 2012, **4**, 810–816.

[74] R. Goeminne, L. Vanduyfhuys, V. Van Speybroeck and T. Verstraelen, *Journal of Chemical Theory and Computation*, 2023, **19**, 6313–6325.

[75] B. Rana, M. P. Coons and J. M. Herbert, *The Journal of Physical Chemistry Letters*, 2022, **13**, 5275–5284.

[76] F. Belleflamme and J. Hutter, *Physical Chemistry Chemical Physics*, 2023, **25**, 20817–20836.

[77] Q. Sun, X. Zhang, S. Banerjee, P. Bao, M. Barbry, N. S. Blunt, N. A. Bogdanov, G. H. Booth, J. Chen, Z.-H. Cui *et al.*, *The Journal of chemical physics*, 2020, **153**, 024109.

[78] F. Weigend and R. Ahlrichs, *Physical Chemistry Chemical Physics*, 2005, **7**, 3297–3305.

[79] F. Weigend, *Journal of computational chemistry*, 2008, **29**, 167–175.

[80] T. H. Dunning Jr, *The Journal of chemical physics*, 1989, **90**, 1007–1023.

[81] J. G. Hill and K. A. Peterson, *The Journal of Chemical Physics*, 2017, **147**, 244106.

[82] A. Nicklass, M. Dolg, H. Stoll and H. Preuss, *The Journal of chemical physics*, 1995, **102**, 8942–8952.

[83] J. Hermann, R. A. DiStasio Jr and A. Tkatchenko, *Chemical Reviews*, 2017, **117**, 4714–4758.

[84] B. Brauer, M. K. Kesharwani, S. Kozuch and J. M. Martin, *Physical Chemistry Chemical Physics*, 2016, **18**, 20905–20925.

[85] S. Jo, T. Kim, V. G. Iyer and W. Im, *Journal of computational chemistry*, 2008, **29**, 1859–1865.

[86] M. Kállay, P. R. Nagy, D. Mester, Z. Rolik, G. Samu, J. Csontos, J. Csóka, P. B. Szabó, L. Gyevi-Nagy, B. Hégely, I. Ladjánszki, L. Szegedy, B. Ladóczki, K. Petrov, M. Farkas, P. D. Mezei and Á. Ganyecz, *J. Chem. Phys.*, 2020, **152**, 074107.

[87] D. Mester, P. R. Nagy, J. Csóka, L. Gyevi-Nagy, P. B. Szabó, R. A. Horváth, K. Petrov, B. Hégely, B. Ladóczki, G. Samu, B. D. Lőrincz and M. Kállay, *J. Phys. Chem. A*, 2025, **129**, 2086.

[88] M. Kállay, P. R. Nagy, D. Mester, L. Gyevi-Nagy, J. Csóka, P. B. Szabó, Z. Rolik, G. Samu, J. Csontos, B. Hégely, Á. Ganyecz, I. Ladjánszki, L. Szegedy, B. Ladóczki, K. Petrov, M. Farkas, P. D. Mezei and R. A. Horváth, MRCC, *a quantum chemical program suite. See*

https://www.mrcc.hu/, Accessed August 1, 2023.
[89] S. F. Boys and F. Bernardi, *Mol. Phys.*, 1970, **19**, 553.
[90] D. Mester, P. R. Nagy and M. Kállay, *J. Chem. Theory Comput.*, 2024, **20**, 7453.
[91] T. H. Dunning Jr., K. A. Peterson and A. K. Wilson, *J. Chem. Phys.*, 2001, **114**, 9244.
[92] T. Helgaker, W. Klopper, H. Koch and J. Noga, *J. Chem. Phys.*, 1997, **106**, 9639.